Supporting Information

Infrared Biosensors Based on Graphene Plasmonics: Modeling

Yuan Zhao,[a] Xiang Hu,[b] Guanxiong Chen,[a] Xuanru Zhang,[b] Ziqi Tan,[a] Junhua Chen,[a]

Rodney S. Ruoff,[c] Yanwu Zhu,*[a] and Yalin Lu*[abd]

[a]Department of Materials Science and Engineering and CAS Key Laboratory of Materials for Energy Conversion, University of Science and Technology of China
96 Jin Zhai Rd, Hefei 230026, China
E-mails: zhuyanwu@ustc.edu.cn (Y. Zhu) and yllu@ustc.edu.cn (Y. Lu)

[b]Advanced Applied Research Center, Hefei National Laboratory for Physical Sciences at the Microscale, University of Science and Technology of China
96 Jin Zhai Rd, Hefei 230026, China

[c]Department of Mechanical Engineering and the Materials Science and Engineering Program, The University of Texas at Austin
One University Station C2200, Austin, TX 78712, United States

[d]Laser Optics Research Center, Physics Department, United States Air Force Academy, CO 80840, USA

Contents

(9). Biosensing based on nearly perfect optical absorption.

Notes and references

(1). Conductivity of graphene

The extraordinary (opto)electronic properties of graphene have been intensively investigated and the conductivity can be adjusted by electrostatic doping (changing the Fermi energy in graphene).[1-5] The conductivity of graphene in the mid-infrared wavelength range modeled with random-phase approximation can be expressed as [6-8]

$$\sigma(\omega) = \frac{2e^2 k_B T}{\pi\hbar^2}\frac{i}{\omega + i\tau^{-1}}\log[2\cosh(E_F/2k_B T)] + \frac{e^2}{4\hbar}[H(\omega/2) + \frac{4i\omega}{\pi}\int_0^\infty d\varepsilon \frac{H(\varepsilon) - H(\omega/2)}{\omega^2 - 4\varepsilon^2}] \quad (1)$$

Where

$$H(\varepsilon) = \frac{\sinh(\hbar\varepsilon/k_B T)}{\cosh(E_F/k_B T) + \cosh(\hbar\varepsilon/k_B T)} \quad (2)$$

The first term corresponds to contributions from intraband transitions and the second term arises from contributions from interband transitions.[8, 9] Here, e is the electronic charge, k_B the Boltzmann constant, $\hbar$ the Planck constant divided by 2π and T the temperature. The analytical expression of graphene conductivity shown above holds for electron and hole bands which exhibit a linear energy dispersion near the zero band-gap points (Dirac points).[10] We restricted our numerical calculations in a wavelength range greater than 3 μm as the linear dispersion relationship can extend into the visible spectrum, shown by a recent experiment.[8, 11] Here, to compute the conductivity of graphene, the following parameters were used: temperature T=300 K, intrinsic relaxation time $\tau=\mu E_F/ev^2_F$, where Fermi energy level E_F (0~0.6 eV), Fermi velocity $v_F\approx10^6$ m/s and moderate carrier mobility $\mu\approx$10 000 cm^2/(V·s) (as μ can range from ~1000 cm^2/(V.s) in chemical vapor deposition synthesized graphene[12] to ~230

000 $cm^2/(V.s)$ in suspended exfoliated graphene.[13] In addition, we has experimentally synthesized graphene with carrier mobility as high as 16 000 $cm^2/(V·s)$ on SiO_2 substrate by chemical vapor deposition (CVD). [14]).

Fig. S1a and b show the real and imaginary part of graphene conductivity, respectively, as a function of Fermi energy level and wavelength in the mid-infrared regime. It can be seen that the conductivity changes with Fermi energy level E_F. In particular, the sign of conductivity imaginary part flips due to the absorption transition because the interband absorption and intraband absorption contribute to the imaginary part of conductivity with different signs.[15] As a result, there is a reversion in the sign of real part of dielectric constant, where "dielectric graphene" is transforming to "metallic graphene".[3, 15] In addition, the plasmonic dispersion property can be tuned by electrical gating due to the massless electrons resting in graphene.[12, 16] As a result, we can tune the resonant wavelength without changing structure parameters. Fig. S1c and d shows the transmission spectra from same structure of p=2w=400 nm but with two different Fermi energy levels of graphene. The resonance wavelength shifts from 7.262 μm for E_F=0.2eV to 4.8 μm for E_F=0.4eV. Fig. S1e shows the local electric field enhancement around graphene-PMMA (polymethyl methacrylate) substrate interface at 7.262 μm for p=2w=400 nm and E_F=0.2eV, with the inset showing the corresponding size of the structure in the lateral direction. The field enhancement is about 28 times at the edge of graphene and decays exponentially with a decay constant of 9.8 nm into the

structure. The intense field enhancement generates strong light-sensing medium interactions, which leads to strong sensing abilities.

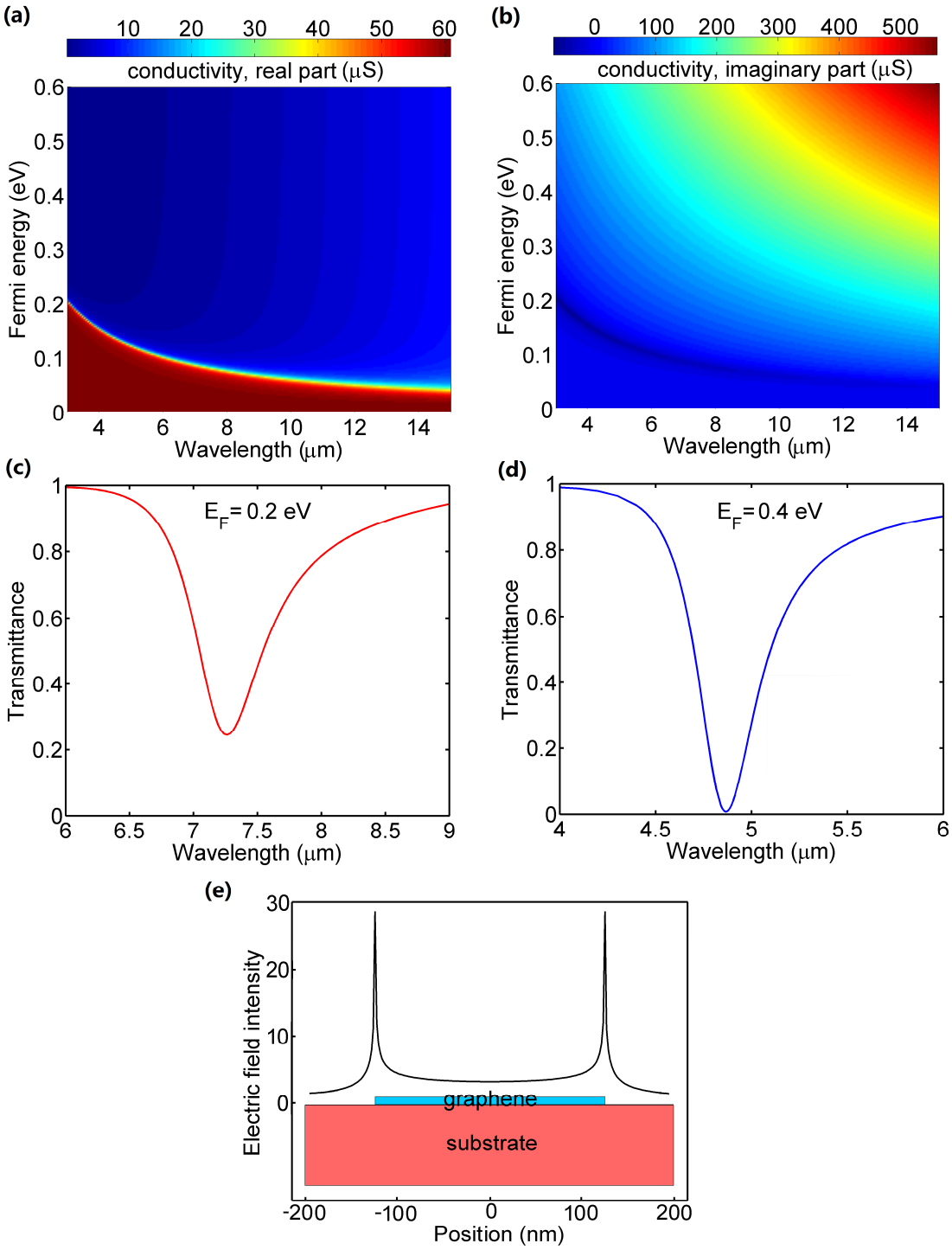

Fig. S1 (a) Real part and (b) imaginary part of the conductivity of graphene as a function of Fermi energy level and wavelength (T=300 K). Simulated transmission spectra with graphene Fermi energy level of (c) 0.2 eV and (d) 0.4 eV, respectively. (e)

Distribution of electric field intensity in the interface between graphene and PMMA substrate as a function of position in the lateral direction at 7.262 μm for p=2w=400 nm and E_F=0.2eV.

(2). Computational method

The proposed structures were simulated with the finite element method using the commercial software Comsol Multiphysics (COMSOL 3.5a), which is a widely accepted method in optics[17-19]. For modeling the structures with two infinite horizontal dimensions, the computational domain was considered as a single unit cell surrounded by either periodic boundary conditions or by perfectly matching layer (PML). The light was incident to the structure surface and the transmittance was calculated from the electromagnetic field distributions obtained.[18]

The wavevector of graphene plasmons is given by[17-19,20]:

$$k_p = \frac{i(\varepsilon_{r1} + \varepsilon_{r2})\varepsilon_0 c}{\sigma} k_0 \qquad (3)$$

Where, k_p is the wavevector of plasmons in graphene, k_0 is the free space wavevector, ε_{r1} and ε_{r2} are dielectric constants of the material above and below the graphene film, respectively, ε_0 is the permittivity of vacuum, c is the velocity of light in the vacuum and σ is the conductivity of graphene.

As the photon energy considered is less than $2E_F$, where E_F is the Fermi energy level of graphene, interband transitions in graphene are forbidden by the Pauli exclusion principle.[7] The conductivity accounting only for intraband transitions can be simplified as[7]:

$$\sigma(\omega) = \frac{e^2 E_F}{\pi\hbar^2} \frac{i}{\omega + i\tau^{-1}} \qquad (4)$$

The resonant wavelength for a nanoribbon width w can be approximated:

$$\lambda_{\mathrm{p}} = 2\eta w \mathrm{Re}(\frac{k_{\mathrm{p}}}{k_0}) = \mathrm{Re}(\frac{2\mathrm{i}c\eta\varepsilon_0(\varepsilon_{\mathrm{r1}}+\varepsilon_{\mathrm{r2}})w}{\sigma}) \quad (5)$$

Where

$$\eta = 2e^2 E_{\mathrm{F}} /(\omega(\omega + \mathrm{i}\tau^{-1})\hbar^2 kw)$$

is a dimensionless constant, which represents the electrodynamic responces of the nanoribbon array and is related to the Fermi energy of graphene, intrinsic relaxation time τ, frequency ω, dielectric constant k of material around graphene and nanoribbon width w. Minimum transmission of incident light takes place at a specific η value, which determines the plasmon resonance frequency ω for given values of E_{F}, τ, k and w.

From Equations (4) and (5), the resonance wavelength is given by[17-19,20]:

$$\lambda_{\mathrm{p}} = \frac{2\pi\hbar c}{e}\sqrt{\frac{\eta\varepsilon_0(\varepsilon_{\mathrm{r1}}+\varepsilon_{\mathrm{r2}})w}{E_{\mathrm{F}}}} \quad (6)$$

In the simulations, the graphene film was modeled as a thin layer of an atom thick with dielectric function $1+4\pi\mathrm{i}\sigma/(\varepsilon_0\omega t)$, where, σ is the surface conductivity, ω is the incident light frequency and t is the graphene layer thickness of 0.34 nm.[20] In the simulations, the dielectric constants of MgF_2, PMMA (polymethyl methacrylate), PS (polystyrene), ion gel, SiO_2, SiC and Si were taken from Refs [12, 21-23]. For modeling the structure used for biosensing, the sensing medium to be detected is placed in direct contact with the structure surface. The biomolecules were modeled as a thin layer adsorbed on graphene nanoribbons in water solutions[24] and their dielectric constants were taken from Refs [25-27].

Firstly, to confirm the feasibility of our simulation method, we compare our simulation results with the experimental data reported in Ref [28] by using the same structure and graphene conductivity (Fig. S2). From the figure, it can be seen that the simulated results are consistent with the reported experimental data and fit well with the modeled curve as well. The agreement of our simulation results with the reported experimental optical spectra enables us to use similar method and conductivity of graphene to predict the optical behavior of graphene plasmons.

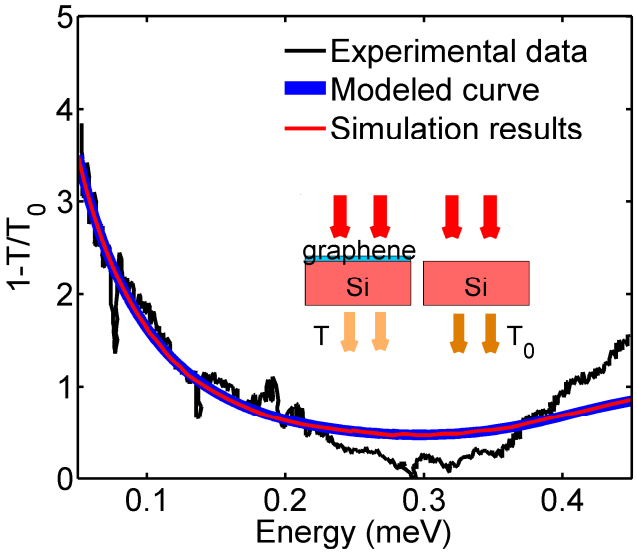

Fig. S2 Transmission spectra for graphene/Si structure (Transmission T) and bare Si substrate (Transmission T_0), respectively. The black line shows experimental data from Ref [29], the blue lines were drawn according to the formula (1) in Ref [29] and the red lines are results obtained by simulation in our work.

(3). Effects of substrate dielectric constants

People have demonstrated that graphene can adsorb biomolecules through the π-stacking interactions between its two dimensional hexagonal cells and the carbon-based ring structures present in biomolecules (e.g., ss-DNA).[29] In addition, the

high surface to volume ratio of graphene provides a large surface area to adsorb biomolecules.[30] As a result, the incorporation of graphene improved the sensitivity in biosensing due to its adsorption.[24] Fig. S3a shows the simulated normal-incidence transmission mapping with varying dielectric constant ε_{r2} of substrate for graphene Fermi energy level E_F of 0.1, 0.2, 0.3 and 0.4 eV, respectively. A wavelength range of 8 μm for each Fermi energy level was selected for comparison. It can be seen that the resonance wavelength shifts to shorter wavelength ranges and the FWHM gets narrower with increase in E_F for same ε_{r2}, which is consistent with Equation 2. Fig. S3b presents the simulated normal-incidence transmission spectra with different substrates when the sensing medium is changing from water (n=1.312) to IgG (human g-immunoglobulin, n=1.41), HSA (human serum albumin, n=1.445),[25] ss-DNA (single-standed DNA, n=1.462), and to ds-DNA (double-standed DNA, n=1.53) in water solutions.[24] Here the Fermi energy level E_F is selected as 0.2 eV and structure parameters of period p=400 nm and nanoribbon width w=200 nm, respectively. To see the detailed effects of the substrates on detecting accuracy and sensitivity and to compare easily, a wavelength range of 0.5 μm for each substrate was selected. We can see that the plasmon resonance shifts to longer wavelength region and the FWHM gets broaden with the increase of dielectric constant of the substrate, indicating decreased detection accuracy. At the same time, the shift of resonance is getting smaller with increase in the dielectric constant of substrate, which results in decreased sensitivity. Also, the change of transmission intensity with a fixed incident wavelength can be used to detect the RI changes of biomolecules. For example, the

sensitivity is 1.2122 RIU^{-1} with fixed incident wavelength of 7.06 μm and PMMA substrate when changing the sensing medium from water to IgG, HSA, ss-DNA, and to ds-DNA in water solutions, respectively.

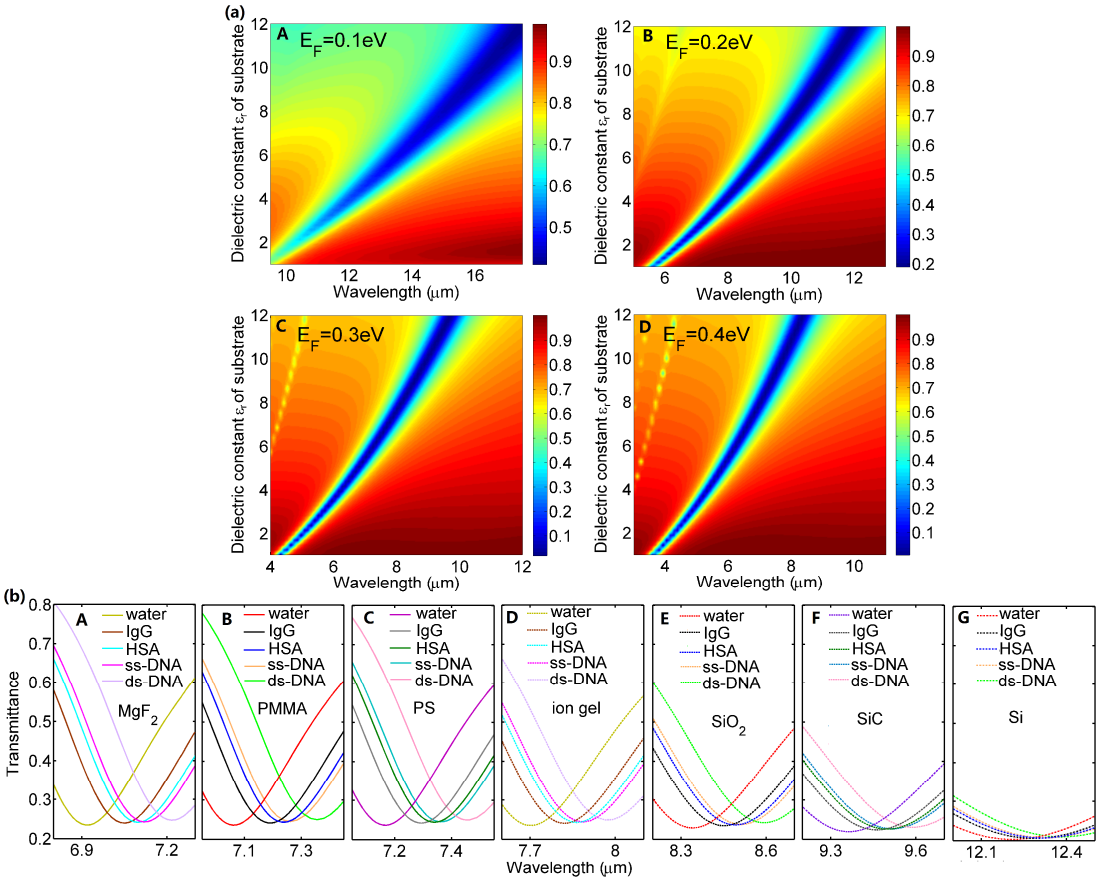

Fig. S3. (a) Simulated normal-incidence transmission mapping with varying dielectric constant ε_{r2} of substrate and incident wavelength for graphene Fermi energy level E_F of 0.1, 0.2, 0.3 and 0.4 eV, respectively when p=2w=400 nm. (b) Simulated normal-incidence transmission spectra when the sensing medium is changing from water to IgG, HSA, ss-DNA, and to ds-DNA in water solutions for MgF_2, PMMA (polymethyl methacrylate), PS (polystyrene), ion gel, SiO_2, SiC and Si substrate, respectively.

(4). Effects of graphene plasmonic structures

Fig. S4a plots the curve of $\lambda_p/w^{1/2}$ as a function of nanoribbon width w. The value of $\lambda_p/w^{1/2}$ is around 0.015 $[m]^{1/2}$, which confirms the predication in the main text. Fig. S4b presents the simulated normal-incidence transmission spectra with three different nanoribbon widths (w=100, 200, 300 nm, respectively) for a fixed period p of 400 nm when changing the sensing medium from water to IgG, HSA, ss-DNA, then to ds-DNA. Here, we fix the wavelength range as 0.6 μm for comparison. We can see the plasmon resonance wavelength red-shifts and gets broaden when increasing the nanoribbon width, leading to decreased detection accuracy.

Fig. S4c shows the simulated normal-incidence transmission spectra (also 0.6 μm range) with four different periods (p=200, 300, 400, 500 nm, respectively) when used for biosensing. We can see the plasmon resonance wavelength red-shifts and gets broaden when increasing the period, resulting in decreased detection accuracy. At the same time, the shift of resonance is getting larger with increased period, which results in increased sensitivity.

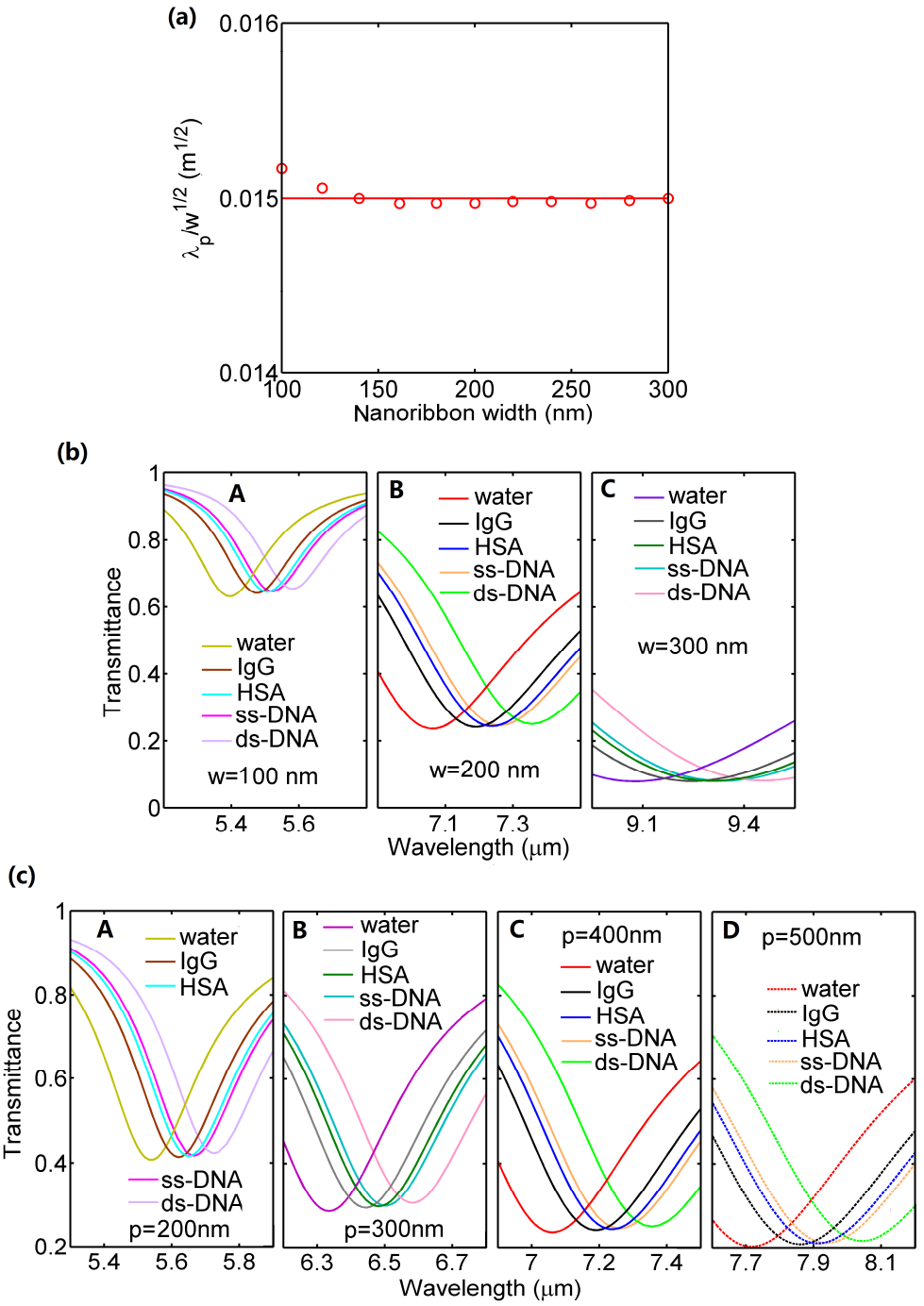

Fig. S4 (a) The function curve of $\lambda_p/w^{1/2}$ with varying nanoribbon width. Simulated normal-incidence transmission spectra when the sensing medium is changing from water to IgG, HSA, ss-DNA, and to ds-DNA for (b) three different nanoribbon widths and (c) four different periods, respectively.

(5). Effects of graphene Fermi energy level

One unique property of plasmonics in graphene is the capability of tuning nanoscale optical field in graphene.[6, 7, 12, 31] The plasmonic spectra can be modulated in a wide wavelength range of from near-infrared to Terahertz (THz) due to the dependence on Fermi energy level.[31] Fig. S5 shows the simulated normal-incidence transmission spectra with different Fermi energy levels when changing the sensing medium from water to IgG, HSA, ss-DNA, then to ds-DNA in water solutions. The structure parameters of period p=300 nm and nanoribbon width w=150 nm were used. The transmission minimum shifts to shorter wavelength and the FWHM gets narrower with the increase of Fermi energy level, indicating increased detection accuracy. At the same time, the sensitivity drops.

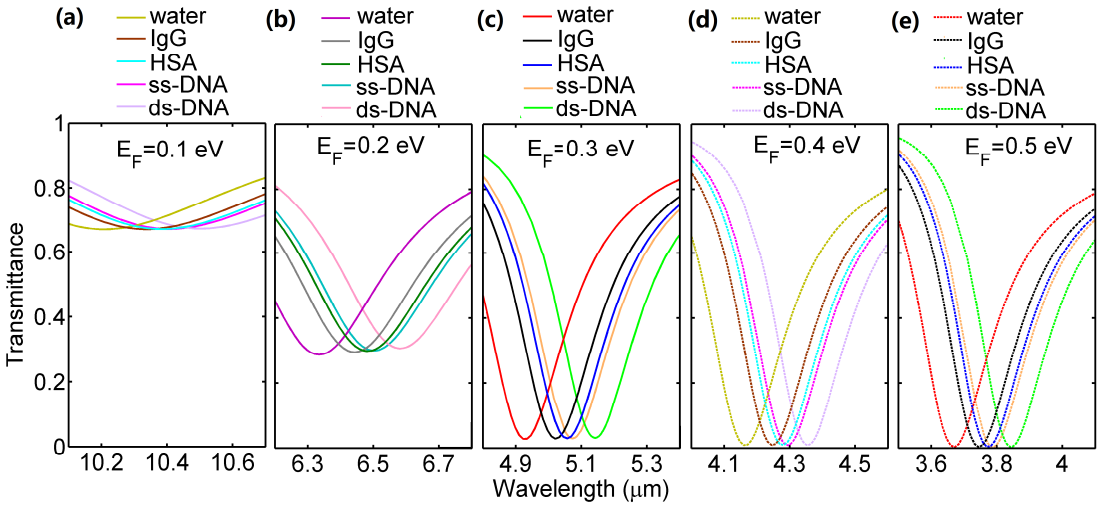

Fig. S5 Simulated normal-incidence transmission spectra when the sensing medium is changing from water to IgG, HSA, ss-DNA, and to ds-DNA for Fermi energy level of (a) 0.1 eV, (b) 0.2 eV, (c) 0.3 eV, (d) 0.4 eV and (e) 0.5 eV, respectively.

(6). Effects of graphene carrier mobility

The resonance properties in the transmission spectra (intensity and line width) are influenced by the optical loss in graphene, which is mainly characterized by the real part of the conductivity of graphene.[7] The low carrier mobility due to the point defects, residue impurity or nanostructure can lead to high loss and large line width.[2, 7, 12] Fig. S6a shows the transmission spectra with different carrier mobilities of graphene; higher carrier mobility of graphene has narrower and deeper transmission notches, indicating increased detection accuracy (Fig. S6c and Fig. S7). However, the sensitivity changes little (Fig. S6b). Hence, the FOM increases (Fig. S6d). It is worth noting that it may be has higher detection accuracy when selecting hexagonal boron nitride (h-BN) as substrate due to higher carrier mobility (as high as 37 000 $cm^2/(V \cdot s)$).[32-34]

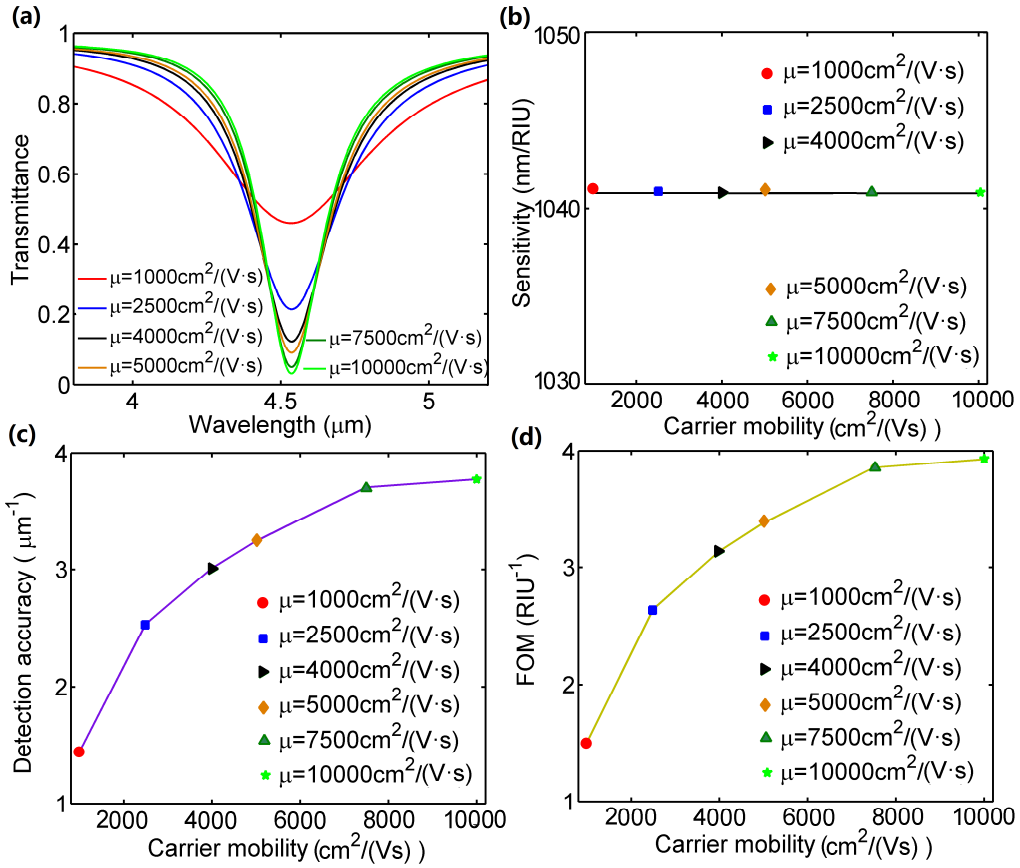

Fig. S6 Graphene plasmonic biosensing with varying carrier mobility of graphene. (a) Simulated normal-incidence transmission spectra and corresponding (b) sensitivity, (c) detection accuracy and (d) FOM for different carrier mobilities when E_F=0.3 eV and p=2w=300 nm.

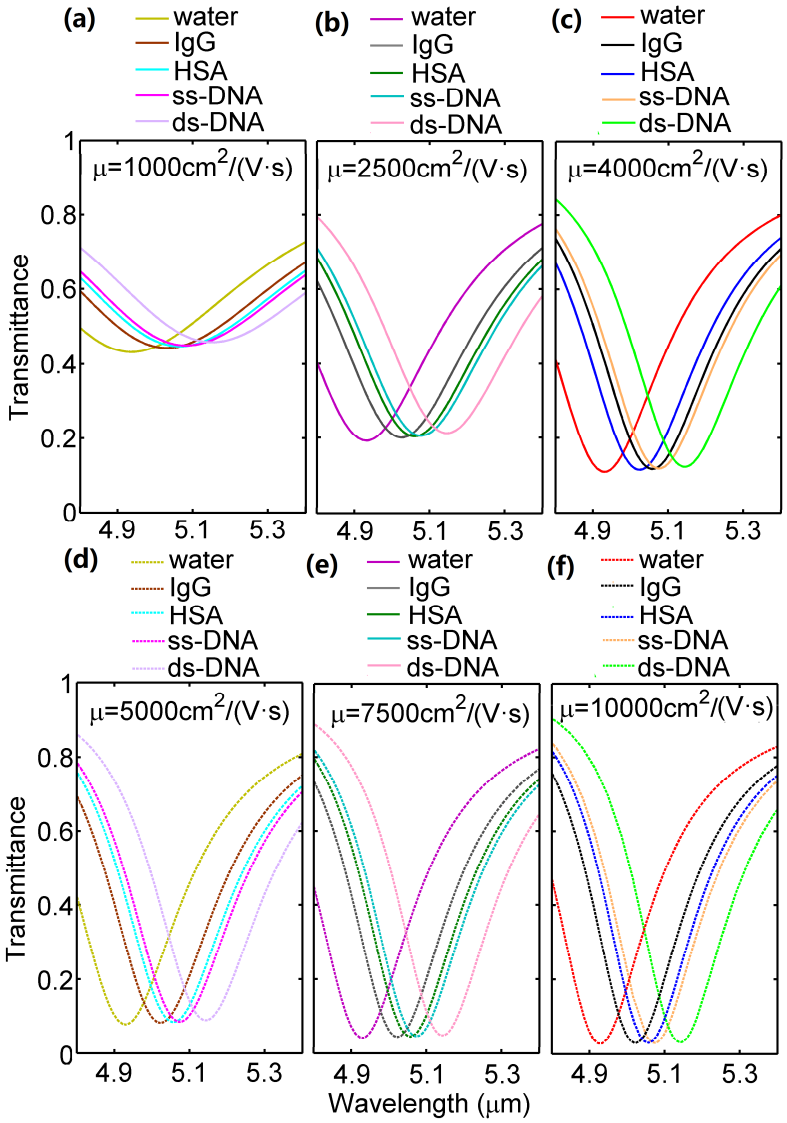

Fig. S7 Simulated normal-incidence transmission spectra when the sensing medium is changing from water to IgG, HSA, ss-DNA, and to ds-DNA for carrier mobility of graphene of (a) 1000 $cm^2/(V·s)$, (b) 2500 $cm^2/(V·s)$, (c) 4000 $cm^2/(V·s)$, (d) 5000 $cm^2/(V·s)$, (e) 7500 $cm^2/(V·s)$ and (f) 10000 $cm^2/(V·s)$, respectively.

(7). Effects of adsorption efficiency (AE) of biomolecules on graphene surface, edge defects and thickness of biomolecule films

The biosensing properties are influenced by the adsorption efficiency (AE, defined as ratio of the adsorption area to the surface area of graphene, i.e. the coverage ratio of molecules on graphene). Fig. S8a shows the simulated normal-incidence

transmission spectra with five different AE values when changing the sensing medium from water to IgG, HSA, ss-DNA, then to ds-DNA in water solutions for E_F=0.3 eV, μ=10000 cm^2/(V·s) and p=2w=300 nm. The shift of transmission minimum gets larger with the increase in the AE value, which indicates increased sensitivity.In the adsorption AE range studied, the FWHM shows little changes. Fig. S8b shows the simulated normal-incidence transmission spectra with varying sensing medium with or without edge defects (edge adsorption). The shift of resonance wavelength is enlarged by edge defects, which benefits biosensing and improves the sensitivity.

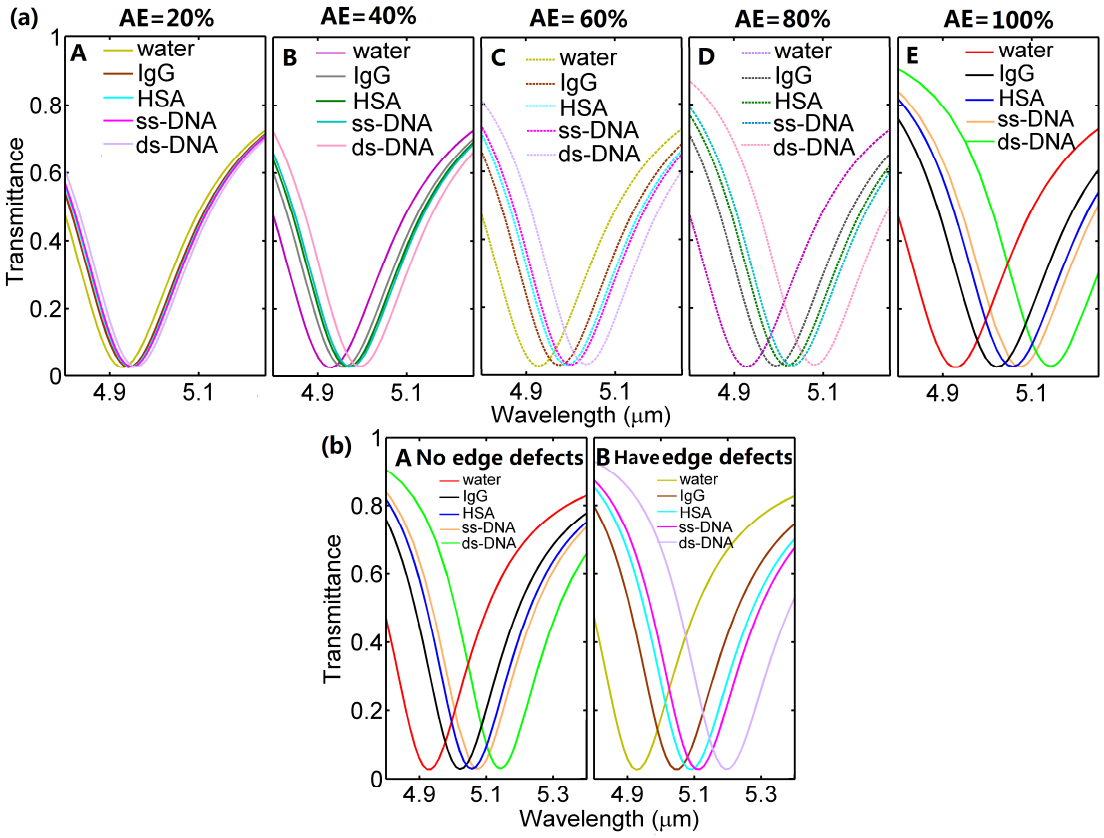

Fig. S8 Simulated normal-incidence transmission spectra when the sensing medium is changing from water to IgG, HSA, ss-DNA, and to ds-DNA for (a) five different AE values and (b) with or without edge defects, respectively.

Fig. S9 shows the simulated normal-incidence transmission spectra with six different thicknesses of the biomolecule films (2, 5, 10, 30, 50 and 100 nm) when changing the sensing medium from water to IgG, HSA, ss-DNA, then to ds-DNA in water solutions. The transmission spectra are similar for the thickness larger than 30 nm. Hence, the sensitivity and detection accuracy wouldn't be significantly affected when varying the thicknesses of the biomolecule films from 30 nm to 100 nm. We also notice that the shift of resonance wavelength for different sensing media could be very weak when the thinness of adsorbed biomolecules is less than 5 nm.

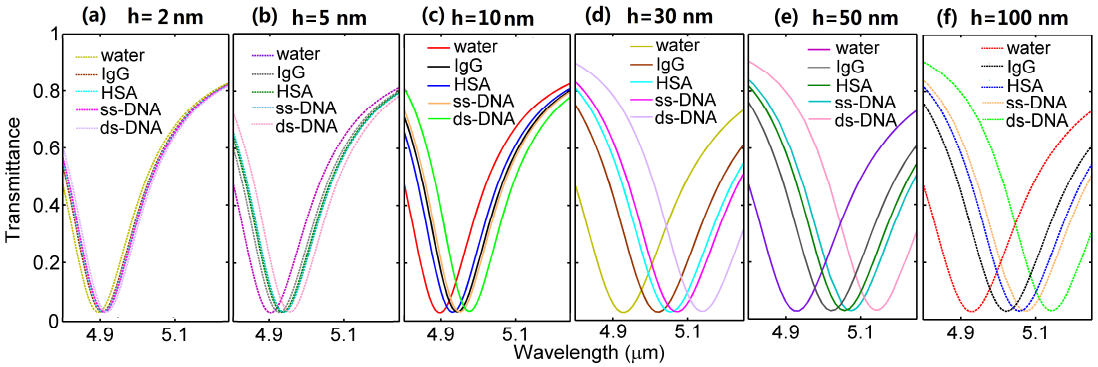

Fig. S9 Simulated normal-incidence transmission spectra when the sensing medium is changing from water to IgG, HSA, ss-DNA, and to ds-DNA for the biomolecule films thickness of (a) 2 nm, (b) 5 nm, (c) 10 nm, (d) 30 nm, (e) 50 nm and (f) 100 nm, respectively.

(8). Effects of rough substrates

To investigate the effect of rough substrate or non-flat graphene, a structure with a layer of graphene in the horizontal direction or both the horizontal and vertical direction each having a layer of graphene was simulated and shown in Fig. S10. To simplify the problem, the vertical graphene has no substrate to support. In fact, it has

found that the calculated result is not sensitive to the height of the vertical graphene. As shown in the transmission spectra, contrast to the normal one transmission minimum for the graphene in the horizontal direction, two transmission minima were observed for the structure consisting of both horizontal and vertical graphene layers. The two transmission dips were considered to be caused by the tips in the vertical direction and the graphene edge in the horizontal direction.[35-38]

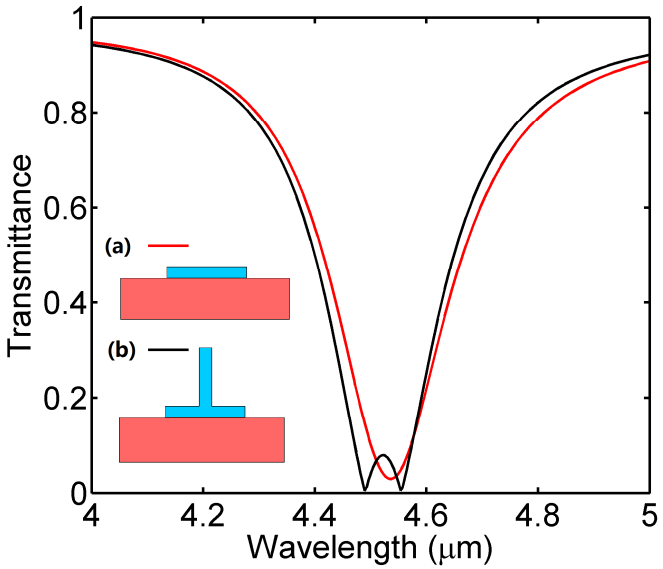

Fig. S10 Simulated normal-incidence transmission spectra for the structure with a layer of graphene in the horizontal direction or both the horizontal and vertical direction each having a layer of graphene, respectively.

(9). Biosensing based on nearly perfect optical absorption.

Recently, complete optical absorption has been investigated with excellent performance in sensing.[39] A nearly perfect optical absorption biosensor device based on graphene plasmonics was also proposed and shown in Fig. S11. Here, a reflection light is detected to response to the sensing medium change. Similarly, high sensitivity values of 1243 and 1394 nm/RIU were obtained from the structures with periods of

300 and 400 nm, respectively (Fig. S11c). Correspondingly, the FOM is 2.98 and 3.11 RIU^{-1}, a little higher than those obtained by detecting transmission spectra with same structure parameters and Fermi energy level (2.82, and 2.37 RIU^{-1} when detecting transmission spectra) due to decreased radiative losses.[6] This structure can be an alternative for being used as graphene plasmonic biosensor.

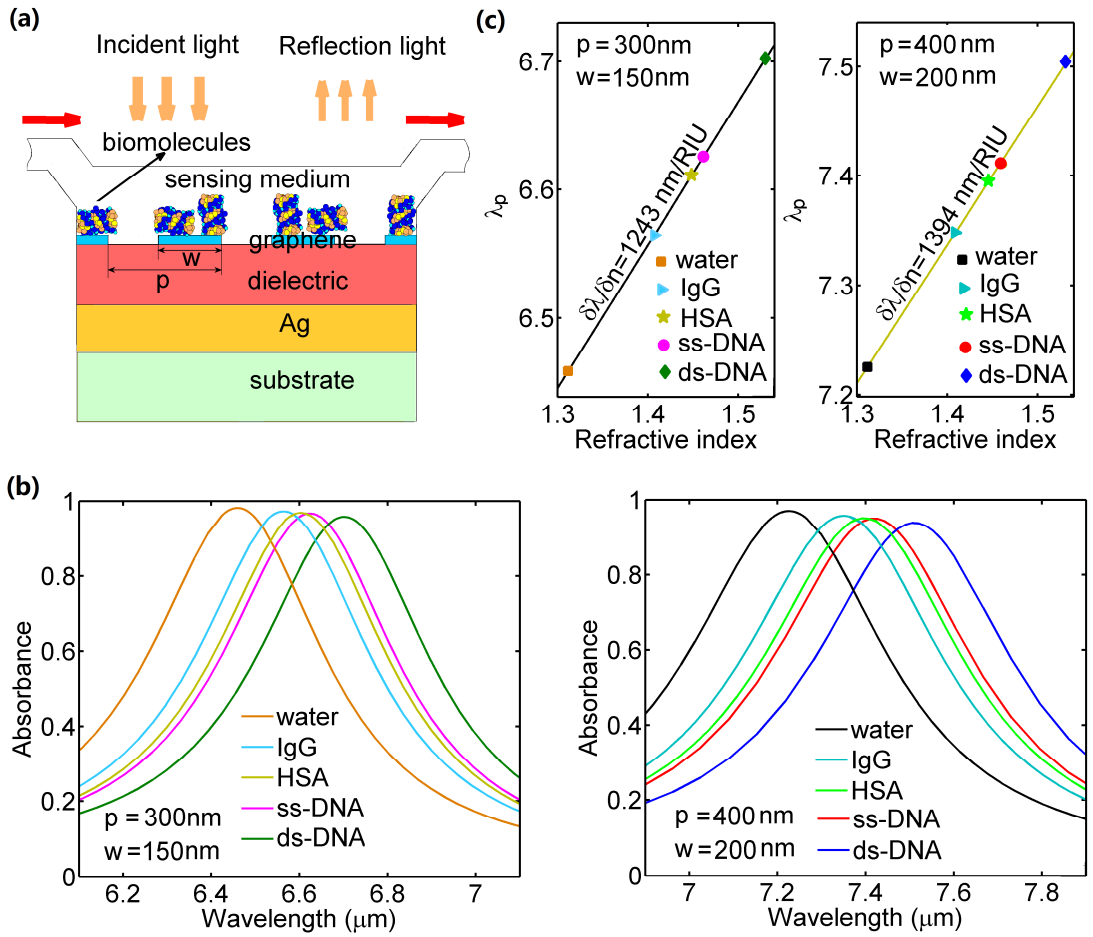

Fig. S11. (a) Schematic of graphene plasmon nearly perfect optical absorption used as biosensor. (b) Simulated normal-incidence absorption spectra with different sensing medium on graphene nanoribbon for p=2w=300 nm and p=2w=400 nm, respectively. (c) The resonance wavelength λ_p versus sensing medium RI curve in a range convering water, ss-DNA and ds-DNA. Dots are simulated data points and lines are linear fits, giving a sensitivity of 1243 nm/RIU and 1394 nm/RIU for period 300 nm

and 400 nm, respectively.

Notes and references

1. Z. Fei, A. S. Rodin, G. O. Andreev, W. Bao, A. S. McLeod, M. Wagner, L. M. Zhang, Z. Zhao, M. Thiemens, G. Dominguez, M. M. Fogler, A. H. C. Neto, C. N. Lau, F. Keilmann and D. N. Basov, *Nature*, 2012, **487**, 82-85.
2. J. Chen, M. Badioli, P. Alonso-Gonzalez, S. Thongrattanasiri, F. Huth, J. Osmond, M. Spasenovic, A. Centeno, A. Pesquera, P. Godignon, A. Zurutuza Elorza, N. Camara, F. Javier Garcia de Abajo, R. Hillenbrand and F. H. L. Koppens, *Nature*, 2012, **487**, 77-81.
3. A. Vakil and N. Engheta, *Science*, 2011, **332**, 1291-1294.
4. F. H. L. Koppens, D. E. Chang, S. Thongrattanasiri and F. J. G. Garcia de Abajo, *OptPN*, 2011, **22**, 36-36.
5. A. H. C. Neto, F. Guinea, N. M. R. Peres, K. S. Novoselov and A. K. Geim, *Rev. Mod. Phys*, 2009, **81**, 109-162.
6. S. Thongrattanasiri, F. H. L. Koppens and F. Javier Garcia de Abajo, *Phys. Rev. Lett.*, 2012, **108**, 047401-047401-047405.
7. W. Gao, J. Shu, C. Qiu and Q. Xu, *Acs Nano*, 2012, **6**, 7806-7813.
8. C. H. Gan, H. S. Chu and E. P. Li, *Phys. Rev. B*, 2012, **85**.
9. L. A. Falkovsky and A. A. Varlamov, *Eur. Phys. J. B*, 2007, **56**, 281-284.
10. L. A. Falkovsky, *Phys-usp*, 2008, **51**, 887-897.
11. R. R. Nair, P. Blake, A. N. Grigorenko, K. S. Novoselov, T. J. Booth, T. Stauber, N. M. R. Peres and A. K. Geim, *Science*, 2008, **320**, 1308-1308.
12. L. Ju, B. Geng, J. Horng, C. Girit, M. Martin, Z. Hao, H. A. Bechtel, X. Liang, A. Zettl, Y. R. Shen and F. Wang, *Nat. Nanotechnol.*, 2011, **6**, 630-634.
13. K. I. Bolotin, K. J. Sikes, Z. Jiang, M. Klima, G. Fudenberg, J. Hone, P. Kim and H. L. Stormer, *Solid State Commun.*, 2008, **146**, 351-355.
14. X. Li, C. W. Magnuson, A. Venugopal, J. An, J. W. Suk, B. Han, M. Borysiak, W. Cai, A. Velamakanni, Y. Zhu, L. Fu, E. M. Vogel, E. Voelkl, L. Colombo and R. S. Ruoff, *Nano Lett.*, 2010, **10**, 4328-4334.
15. Z. Lu and W. Zhao, *J. Opt. Soc. Am. B: Opt. Phys.*, 2012, **29**, 1490-1496.
16. C. Chi-Fan, P. Cheol-Hwan, B. W. Boudouris, J. Horng, G. Baisong, C. Girit, A. Zettl, M. F. Crommie, R. A. Segalman, S. G. Louie and W. Feng, *Nature*, 2011, **471**, 617-620.
17. A. V. Krasavin and A. V. Zayats, *Phys. Rev. B (Condensed Matter and Materials Physics)*, 2008, **78**, 045425-045421-045428.
18. T. Holmgaard and S. I. Bozhevolnyi, *Phys. Rev. B*, 2007, **75**, 245405 (245401-245412).
19. B. Yun, G. Hu and Y. Cui, *Opt. Express*, 2009, **17**, 3610-3618.
20. L. Wu, H. S. Chu, W. S. Koh and E. P. Li, *Opt. Express*, 2010, **18**, 14395-14400.
21. J. M. Siqueiros, R. Machorro and L. E. Regalado, *Appl. Optics.*, 1988, **27**, 2549-2553.
22. E. D. Palik., *Academic Press*, 1985.
23. R. T. Graf, J. L. Koenig and H. Ishida, *Appl. Spectrosc.*, 1985, **39**, 405-408.
24. S. H. Choi, Y. L. Kim and K. M. Byun, *Opt. Express*, 2011, **19**, 458-466.
25. J. Voros, *Biophys. J.*, 2004, **87**, 553-561.
26. D. E. Gray, S. C. CaseGreen, T. S. Fell, P. J. Dobson and E. M. Southern, *Langmuir*, 1997,

13, 2833-2842.

27. G. M. Hale and M. R. Querry, *Appl. Optics.*, 1973, **12**, 555-563.
28. S. Mou, S. S. Kim, K.-H. Chen, L.-C. Chen, R. R. Naik, G. J. Brown and W. C. Mitchel, *SPIE Proceedings*., 2012, 8462.
29. C.-H. Lu, H.-H. Yang, C.-L. Zhu, X. Chen and G.-N. Chen, *Angew. Chem. Int. Edit.*, 2009, **48**, 4785-4787.
30. P. K. Maharana and R. Jha, *Sensor Actuat. B-chem*, 2012, **169**, 161-166.
31. J. Christensen, A. Manjavacas, S. Thongrattanasiri, F. H. L. Koppens and F. Javier Garcia de Abajo, *Acs Nano*, 2012, **6**, 431-440.
32. N. O. Weiss, H. Zhou, L. Liao, Y. Liu, S. Jiang, Y. Huang and X. Duan, *Adv. Mater.* , 2012, **24**, 5782-5825.
33. J. Chan, A. Venugopal, A. Pirkle, S. McDonnell, D. Hinojos, C. W. Magnuson, R. S. Ruoff, L. Colombo, R. M. Wallace and E. M. Vogel, *Acs Nano*, 2012, **6**, 3224-3229.
34. W. Gannett, W. Regan, K. Watanabe, T. Taniguchi, M. F. Crommie and A. Zettl, *Appl. Phys. Lett.*, 2011, **98**.
35. C. L. Nehl, H. W. Liao and J. H. Hafner, *Nano Lett.*, 2006, **6**, 683-688.
36. S. Eustis and M. A. El-Sayed, *J. Appl. Phys.*, 2006, **100**, 044324-044321-044327.
37. T. K. Sarma and A. Chattopadhyay, *Langmuir*, 2004, **20**, 3520-3524.
38. V. Amendola, O. M. Bakr and F. Stellacci, *Plasmonics*, 2010, **5**, 85-97.
39. N. Liu, M. Mesch, T. Weiss, M. Hentschel and H. Giessen, *Nano Lett.*, 2010, **10**, 2342-2348.